Materials and Design 156 (2018) 494–503

Contents lists available at ScienceDirect

Materials and Design

journal homepage: www.elsevier.com/locate/matdes

Light-based additive manufacturing of PolyHIPEs: Controlling the surface porosity for 3D cell culture applications

Colin Sherborne [a,1], Robert Owen [b,1], Gwendolen C. Reilly [b], Frederik Claeyssens [a,*]

[a] The Kroto Research Institute, North Campus, University of Sheffield, Broad Lane, Sheffield S3 7HQ, United Kingdom
[b] Department of Materials Science and Engineering, INSIGNEO Institute for in silico medicine, The Pam Liversidge Building (C+04), Sir Frederick Mappin Building, Mappin Street, Sheffield S1 3JD, United Kingdom

HIGHLIGHTS

- UV-234 (commercially Tinuvin®234) addition is beneficial when printing inherently porous tissue engineering constructs via stereolithography.
- Formation of PolyHIPE surface skin during stereolithography is reduced by adding UV-234 to the monomer phase.
- UV-234 reduces the cured area of the PolyHIPE, permitting higher resolution structures to be produced with smaller spacing.
- UV-234 PolyHIPEs were non-toxic and supported improved osteoblast activity showing their great prospects in 3D cell culture.

GRAPHICAL ABSTRACT

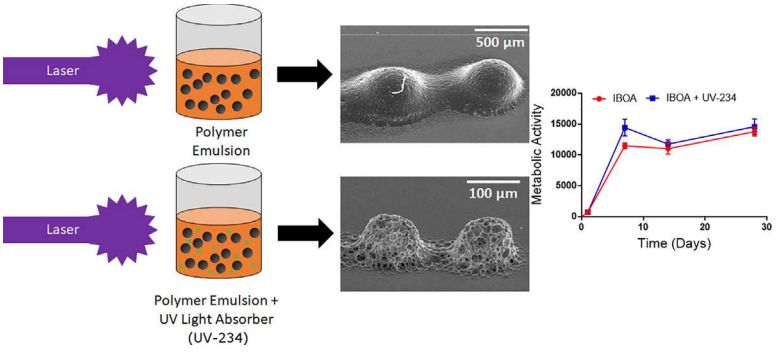

ARTICLE INFO

Article history:
Received 10 May 2018
Received in revised form 28 June 2018
Accepted 29 June 2018
Available online 4 July 2018

Keywords:
Bone tissue engineering
PolyHIPE
Emulsion templating
Vat photopolymerisation
Stereolithography
3D cell culture
Tinuvin

ABSTRACT

Using stereolithography (vat photopolymerisation) to polymerise High Internal Phase Emulsions (PolyHIPEs) is a potent additive manufacturing route to produce materials with a hierarchical porosity. These multiscale porous materials have a microporosity (1–50 μm) dictated by emulsion templating and a macroporosity (100 μm upwards) controlled by additive manufacturing. The interconnected, hierarchical porosity of these structures is particularly desirable in the field of bone tissue engineering as it promotes tissue formation and allows efficient mass transport. However, due to the high light-scattering nature of the HIPEs, the achievable feature resolution is poor in comparison to other photocurable polymers, and they are prone to the formation of a closed porosity 'skin layer' at the surface. This study focuses on different methods of both improving the resolution of structures fabricated from HIPEs via stereolithography and minimising skin formation. The inclusion of 2-(2H-Benzotriazol-2-yl)-4,6-bis(1-methyl-1-phenylethyl)phenol (commercially UV-234 or Tinuvin®234), a UV light-absorber, was found to significantly improve the achievable resolution of PolyHIPE structures fabricated via stereolithography with no cytotoxic effects and reduce the skin formation. Furthermore, in direct comparison with a non-microporous scaffold of the same architecture, the inclusion of a microporosity significantly promoted the proliferation of MLO-A5 murine osteoblasts and permitted superior bone-matrix deposition.

* Corresponding author at: Department of Materials Science and Engineering, University of Sheffield, Kroto Research Institute, Broad Lane, Sheffield S3 7HQ, United Kingdom.
E-mail address: f.claeyssens@sheffield.ac.uk (F. Claeyssens).
[1] Joint first authors.

https://doi.org/10.1016/j.matdes.2018.06.061

1. Introduction

Synthetic biomaterials that can be structured into porous scaffolds to support cell growth have played an influential role in developing the field of tissue engineering [1]. An emerging research interest in this area is the combination of additive manufacturing technologies and emulsion templating to produce multiscale porosity materials [2–4]. A high level of pore interconnectivity and percentage porosity are essential requirements for a tissue engineering scaffold as they permit sufficient oxygen and nutrient transfer to support the growth and proliferation of cells [5], and emulsion templating is an appealing method to incorporate these requirements into the scaffold due to the ease with which interconnected porosity can be generated [6].

To achieve this, an emulsion is created where a typically hydrophobic pre-polymer is mixed with water and a suitable surfactant; this mixture of immiscible liquids creates a suspension of water droplets surrounded by a continuous pre-polymer phase. When the droplet phase exceeds 74% of the total volume the emulsion is classified as a High Internal Phase Emulsion (HIPE) [7]. By polymerising the continuous phase through gelling and crosslinking the pre-polymer component within this emulsion, the three-dimensional (3D) structure of the emulsion is preserved whilst the water is removed, and the resulting scaffold is known as a PolyHIPE [19].

The pre-processing conditions of the emulsion directly affect the PolyHIPE morphology. Very high porosity can be achieved by increasing the droplet volume ratio in the emulsion, with ratios of up to 99% being reported [8]. Varying the surfactant concentration affects both the emulsion stability and the pore interconnectivity [9]. Furthermore, the preferential solubility of the initiator into the internal or continuous phase can determine whether open or closed porosity scaffolds are created [10]. A range of polymer materials have been used with this fabrication method [11,12], enabling the production of a new generation of scaffold materials for 3D cell culture and tissue engineering constructs [13–16].

The choice of materials with which one can create a biodegradable PolyHIPE is limited to sufficiently hydrophobic monomers to create the initial water-in-oil emulsion. Despite this, thermally cured biodegradable monomers such as poly(lactic acid) [17], and propylene fumarate dimethacrylate (PFDMA) exist [18]. Photocurable biodegradable thiol-ene based PolyHIPEs containig a PCL-triacrylate have also been developed by Cameron et al. [19].

There are currently two additive manufacturing techniques that have been combined with light initiated emulsion templating: stereolithography (vat photopolymerisation) and materials extrusion (fused deposition modelling, robocasting or slurry dispensing). In stereolithography the photocurable resin is cross linked via spatially resolved exposure to ultraviolet (UV) light. This can be combined with emulsion templating either by using dynamic mask projection [2], or by directly scanning the UV light to polymerise the emulsion [3,4,13]. During materials extrusion an emulsion ink is extruded through a syringe and the emulsion sets afterwards via a thermal or UV initiated polymerisation [15]. Emulsion templating is ideally suited to produce a resin for these techniques because its viscosity can be modulated; the viscosity of the HIPEs can be low enough for sufficient surface spreading for stereolithography [3,4] or high enough to retain its shape during extrusion via addition of high viscosity additives or high speed mixing [15,20]. In all cases, the microporosity of the polyHIPE can be controlled independently from the macroporosity, which is produced by additive manufacturing.

The microporosity within polyHIPEs can range from 1 to 100 μm depending on the initial emulsion formulation [7]. This distribution encompasses the ideal feature size range for cell ingrowth and proliferation, making them excellent scaffolds for 3D cell culture. 3D tissue culture has been observed on porous disks of these materials for a range of cell types and applications, including cartilage regeneration [6], proliferation of human fibroblasts [17], neuronal cells [21], and osteoblasts [10,18,22]. The pore size and interconnectivity is a crucial factor for cell ingrowth and 3D tissue generation [23]. Additionally, structuring of these PolyHIPEs via stereolithography was previously demonstrated to enable fabrication of a range of structures with hierarchical porosity [2,3,24]. Previous work within our group has developed PolyHIPE based porous woodpile structures for bone tissue engineering applications, focusing on incorporating hydroxyapatite and implementing tunable mechanical properties [4,13].

This photopolymerisation technique for 3D printing bone tissue engineering scaffolds is not the only method utilised recently to progress the field. For example, other groups have employed extrusion-based techniques to create woodpile structures from a range of polymer (e.g. PLA, PCL) and composite materials (e.g. PCL/hydroxyapatite) [25,26]. Fused deposition modelling has been used to produce gyroid scaffolds from PLA [27], and alginate/gelatin bio-inks with nano-hydroxyapatite coatings have also been developed to create composite scaffolds [28]. In a similar fashion, the osteoconductive properties of biodegradable PolyHIPE scaffolds can be improved by the addition of amorphous calcium phosphate nanoparticles [29], or by hydroxyapatite and strontium-modified hydroxyapatite [30] during the emulsion stage.

In comparison to other methods, a key advantage of this emulsion templating technique is the ease with which a microporosity within scaffold fibres that can be included and controlled. Despite this, a limitation of using a HIPE as a photocurable resin for stereolithography is its highly light scattering nature. This scattering has a pronounced effect on the maximum achievable feature resolution, reducing it in comparison to non-emulsified pre-polymers. Furthermore, it also can result in a closed surface porosity due to the formation of a surface 'skin', negating the benefits of the highly porous PolyHIPE material.

In this study we assess the consequences of this light scattering on the achievable feature resolution and surface skin formation, and determine to what extent inclusion of light absorbers can mitigate it. Any potential cytotoxicity was subsequently evaluated by culturing the murine osteoblast cell line MLO-A5 on PolyHIPE scaffolds produced with or without the light absorber, and comparing cell viability. Finally, PolyHIPE scaffolds were compared to a commercial product that had a similar-macroscopic architecture but lacked the inherent microporosity of the PolyHIPE material, thereby allowing the potential advantages of using HIPEs as resins for stereolithography in the field of bone tissue engineering to be assessed.

2. Materials and methods

All solvents mentioned in the methods are reagent grade and purchased from Sigma-Aldrich (Poole, UK) unless otherwise mentioned.

2.1. HIPE synthesis

PolyHIPEs were fabricated from isobornyl acrylate (IBOA) based HIPEs. The continuous phase was formed from two organic components; IBOA and a crosslinker (trimethylolpropane triacrylate (TMPTA) added at 26.96 wt% of the IBOA. A surfactant, Hypermer B246-SO-(MV) (kindly donated by Croda, UK), was added at 3 wt% of the organic components and left to dissolve in a sonic water bath. Finally, a photoinitiator (2,4,6-trimethylbenzoyl)-phosphine oxide/2-hydroxy-2-methylpropiophenone, 50/50) was added at 5 wt% of the organic components. If the composition included the light-absorber, 2-(2H-Benzotriazol-2-yl)-4,6-bis(1-methyl-1-phenylethyl)phenol (UV-234, commercially known as Tinuvin®234), it was added with the surfactant. HIPEs of 80% porosity were formed through the dropwise addition of the internal phase (distilled water) to the continuous phase whilst stirring at 350 rpm (Pro40, SciQuip). IBOA PolyHIPEs are referred to as either 'IBOA' or 'IBOA+UV-234' if they contain the light-absorber.

2.2. PolyHIPE scaffold fabrication

The stereolithography setup consisted of a sub-nanosecond pulse duration, passively Q-switched DPSS microchip laser (PULSELAS-P355-300, ALPHALAS, Germany), controlled using a laser diode and thermo-electric cooler driver (LDD1-1BT-D, ALPHALAS, Germany), emitting wavelengths of 1064, 532 and 355 nm was used as the light source. A Pellin–Broca prism (ADB-10, Thorlabs, UK) was used to separate a single wavelength of 355 nm. Beam delivery was controlled with a shutter (UNIBLITZ LS6, Vincent Associates, Canada) linked to a shutter driver (VCM-D1, Vincent Associates, Canada). The beam was focused through a microscope objective (EC-Plan NEOFLUAR 10×, Carl Zeiss Ltd., UK). A high precision translation stage ANT130-XY (Aerotech, UK) for *xy*-translation & PRO115 (Aerotech, UK) for *z*-translation, controlled by software (A3200 Software-Based Machine Controlled (Aerotech, UK)) was used to scan the focal spot through the resin. The laser was focused just above the coverslip-HIPE interface for the bottom layer and the fibre-HIPE interface for each subsequent layer in order to write the scaffold.

Four-layer circular woodpile scaffolds were fabricated following the protocols described in [4]. In this study, we used untreated coverslips for all scaffolds to ensure it could be removed from the glass base, creating a free-standing scaffold. For compositions without UV-234, the UV power was measured to be 1–5 mW directly after the objective (using a PM100D power meter, with a S310C thermal sensor, Thorlabs). When compositions contained the light-absorber, the power was set to 5 mW. To create the scaffold, a layer of HIPE was pipetted onto the coverslip attached to a glass slide mounted on the stage and the first layer fabricated. Additional HIPE was added after the completion of each layer. Once completed, scaffolds were washed with acetone and air dried.

2.3. Mechanical characterisation

Sheets of IBOA or IBOA + UV-234 PolyHIPE were fabricated and cut into tensile specimens in accordance with the protocol developed by Owen, et al. [31]. Briefly, HIPE was pipetted into a silicone mould and cured using a UV spot curer for 30 s at 100 W [Omnicure S1500, Excelitas Technologies] before washing in acetone overnight and drying. Sheets were laser cut (Mini 18 Laser, Epilog Laser) to a test shape in accordance with a modified version of ASTM D638-10. Specimens were tested on a TA Instruments ElectroForce 3200 using a 450 N load cell, an extension rate of 0.02 mm/s, a grip distance of 10 mm, and a maximum extension of 10 mm. The Young's Modulus of each sample was determined using the gradient of the linear-elastic region of the force displacement curve, with the first point taken at 0.02 mm and the final at yield.

2.4. Scanning electron microscopy

A Philips XL-20 SEM was used to image the PolyHIPE samples. All samples were sputter coated with gold to improve surface conductivity before SEM imaging. We estimated the average pore size of the PolyHIPE by measuring 150 pores and multiplying them by the statistical correction factor $2/\sqrt{3}$. This is because the measured values are an underestimate of the true pore diameters due to the uneven sectioning through the pores [32].

2.5. General cell culture

MLO-A5, a murine osteoblast cell line, (kindly donated by Dr. Lynda Bonewald, University of Missouri) was selected for cell culture testing due to its previous use in evaluating bone tissue engineering scaffolds [33, 34]. They were expanded at 37 °C, 5% CO_2 in basal media (BM), containing Minimum Essential Alpha Medium (α-MEM, Lonza, UK), 10% foetal bovine serum (FBS, Labtech, UK), 2 mM L-glutamine (Sigma Aldrich, UK) and 100 mg/mL penicillin/streptomycin (Sigma Aldrich, UK) in gelatine-coated T75 flasks until ~90% confluent. During passage, media was changed every 2–3 days. Cells were used between the 34th and 39th passage, supplemented media (SM), was added from day 1.

PolyHIPE scaffolds were sterilised by submerging in 70 vol% ethanol for 90 min before rinsing three times in sterile PBS. They were then soaked in Basal Medium (BM) for 30 min prior to seeding. For cell seeding suspension of 25,000 cells at a concentration of 250,000 cells/mL was added to the BM soaking the scaffolds and orbitally shaken at 50 rpm for 45 min to disperse the cells throughout the scaffold. Cultures were left overnight in BM and the following day replaced with supplemented media (SM) consisting of BM with 5 mM beta-glycerolphosphate (βGP) and 50 μg/mL ascorbic acid 2-phosphate (AA2P). Media was changed every 2–3 days.

2.6. Cell viability assays

To evaluate cell viability, resazurin reduction (RR) assays were performed. Resazurin sodium salt is reduced to resorufin by metabolically active cells, changing the colour of the media from a non-fluorescent blue to a highly fluorescent pink. The intensity of the fluorescence is correlated with metabolic activity. A RR working solution was made by dissolving 10 vol% resazurin stock solution (1 mM resazurin sodium salt in diH_2O) in BM. To perform the assay, scaffolds were transferred to a new well plate before adding 1 mL of the working solution to ensure only cells adhered to the scaffold were analysed. The well plate was then wrapped in aluminium foil and incubated for 4 h under standard conditions. 200 μL of the reduced solution was transferred in triplicate to a 96-well plate and read on a plate reader (Tecan infinite 200-pro) at λ_{ex}: 540 nm and λ_{em}: 590 nm. Finally, scaffolds were washed twice with PBS to elute any residual RR before adding fresh media.

2.7. Calcium and collagen quantification

The extracellular matrix deposited by osteoblasts contains an inorganic mineral phase containing calcium, and an organic phase predominantly consisting of collagen. By analysing calcium and collagen deposition, the amount of bone-like tissue that has been deposited can be ascertained. Samples were fixed prior to calcium and collagen quantification by removing the media, washing twice with PBS, and submerging in 3.7% formaldehyde for 30 min. The fixative was then removed and the samples washed twice in deionised water (diH_2O).

Calcium quantification was performed by Alizarin Red S (ARS) staining. ARS was dissolved at 1 w/v% in diH_2O. The solution was filtered using a 0.45 μm to remove undissolved particulates and the pH adjusted to 4.1. Samples were submerged in a known volume of the stain and left for 30 min. The stain was then removed and the samples washed with diH_2O every 5 min whilst orbitally shaking at 100 rpm until the wash-water remained clear. A known volume of 5% perchloric acid was then added to destain the samples and left on the orbital shaker at 100 rpm for 15 min. 150 μL was then transferred in triplicate to a 96 well plate and read at an absorbance of 405 nm. (Tecan infinite 200-pro). The concentration of ARS was determined via a standard curve created by serially diluting the staining solution in the destain. From this, the absorbance units can be converted to a quantity of ARS.

Collagen production was evaluated by Direct Red 80 (DR80) staining. Similar to ARS, it can also be destained and quantified. DR80 was dissolved in saturated picric acid at 1 w/v%. The solution was filtered using a 0.45 μm to remove undissolved particulates. Samples were submerged in a known volume of DR80 stain and left for 18 h on an orbital shaker at 100 rpm. The staining solution was then removed and the samples washed with diH2O every 5 min whilst orbitally shaking at 100 rpm until the wash-water remained clear. A known volume of 0.2 M NaOH and MeOH in a 1:1 ratio was then added to destain the samples and left on the orbital shaker at 100 rpm for 20 min. 150 μL was

then transferred in triplicate to a 96 well plate and read at an absorbance of 405 nm. (Tecan infinite 200-pro). The concentration of DR80 was determined via a standard curve created by serially diluting the staining solution in the destain. From this, the absorbance units can be converted to a quantity of DR80.

2.8. Statistical analysis

All statistical analysis was undertaken in Graphpad Prism (version 7.00). Data was analysed by two-way analysis of variance (ANOVA) with Tukey's multiple comparisons test to evaluate significant differences. Differences were considered significant when $p < 0.05$. All graphs are presented as mean ± standard deviation unless otherwise stated and notable significant differences are indicated on the graphs or in the legends. All experiments were performed a minimum of two times in triplicate for each condition. The total number of replicates (n) is stated in the figure legend.

3. Results

3.1. Laser scan speed affects the resolution and quality of polymerised features

Increasing the laser scan speed decreased the width of the polymerised lines. A series of 8 lines, 2 mm long and spaced 1 mm apart were polymerised at different speeds by scanning the laser light (5 mW) focused onto the IBOA emulsion/glass interface from underneath the coverslip. The laser scan speed for each line was increased in increments of 0.5 mm/s. The width of the polymerised lines decreased as the laser scan speed was increased from 0.5 to 1.0 and 1.5 mm/s (Fig. 1C). Laser scan speeds 3.5 mm/s and above resulted in in a very thin polymer being formed on the glass surface (Supplementary Fig. S1).

There was a polymer skin on the side of all the PolyHIPE lines. No polymer skin or closed pored surface was found on the top of the PolyHIPE lines polymerised with a slow scan speed of 0.5 and 1 mm/s. The top surface for these write speeds was cured against air while the side surface has cured against the surrounding emulsion (see Fig. 1A–B). The features were cut with a scalpel and imaged by SEM. The surface skin of polymer was only observed on the outer surface of the lines. All polymerised lines retained an internal PolyHIPE morphology (Fig. 1C).

The two lines written at the slowest speeds (0.5 and 1 mm/s) were abridged by a layer of cross-linked polymer (Fig. 1C). This overcuring effect was not observed between the lines written at the faster fabrication speeds (above 1.5 mm/s). A polymer residue was present on the glass surface between the polymerised lines and surrounded the base of the PolyHIPE lines.

3.2. Laser light scattering produces connecting polymer strands/bridges

To determine parameters where overcuring occurs, a 10 × 12 dot array was produced with the laser at a constant spacing of 700 μm to produce 120 polymerised PolyHIPE protrusions. The laser exposure time was increased from 0.01–1.30 s in increments of 0.01 s which resulted in the polymerised regions gradually increasing in size, and eventually merging together (Fig. 2).

As when fabricating the lines, the PolyHIPE protrusions had a closed outer skin layer. These can be seen from the high magnification SEM images (Fig. 2B–D). This thin layer of polymer was also found on the glass surface between and around the protrusions and in line with the connecting polymer bridges (Fig. 2C–D). When the laser exposure duration exceeded 0.79–0.82 s, at a spacing of 700 μm, straight, well defined polymer bridges formed between the protrusions.

The formation of these polymer bridges was highly controllable and determined by the pulse duration and distance between the protrusions (Supplementary Fig. S2). From Fig. 2C, it was determined that the polymer bridges start to form when the distance between the protrusions is twice their diameter. As the laser exposure time was further increased (0.8–1.3 s), all the polymer protrusions gradually merged together to form an 'egg-box' like structure. The polymer bridges are caused by the high light scattering nature of the emulsions during photopolymerisation (as further indicated by Section 3.3). This scattering

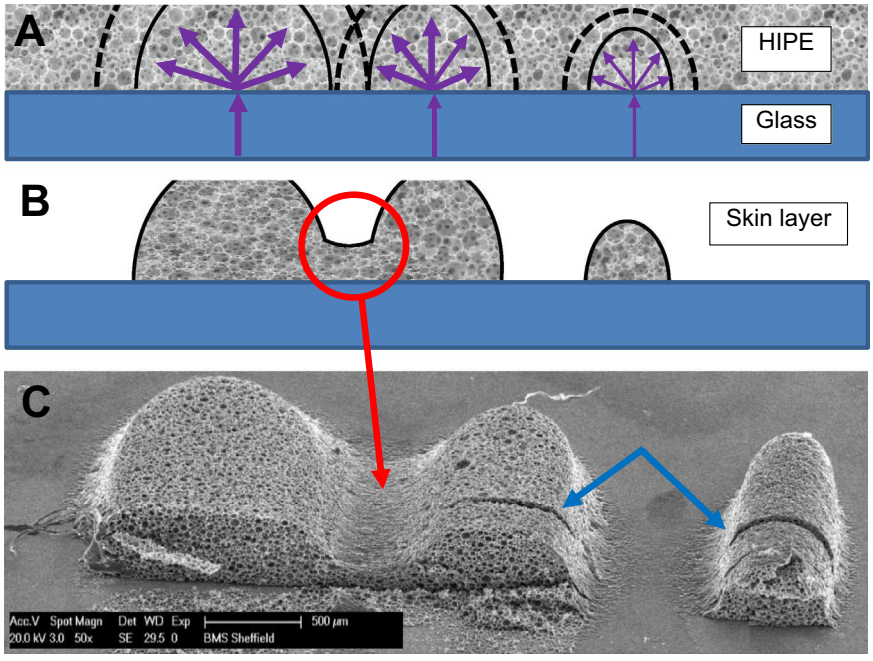

Fig. 1. (C) SEM images of PolyHIPE lines polymerised on top of a glass coverslip at (left to right) 0.5, 1.0 and 1.5 mm/s. Lines have been cut in half to view their internal morphology. Overcuring (red arrow) occurs between the 0.5 and 1.0 mm/s line. A 'side skin' can be seen on the lateral surfaces of the lines (blue arrow). (B) Diagram showing the overcuring effect. The black line shows where the surface skin is present (A) Diagram showing how increased light scattering (purple arrows) at lower laser scan speeds causes overcuring. The solid line shows the curing region while the dashed line indicates the boundary of the partially crosslinked emulsion.

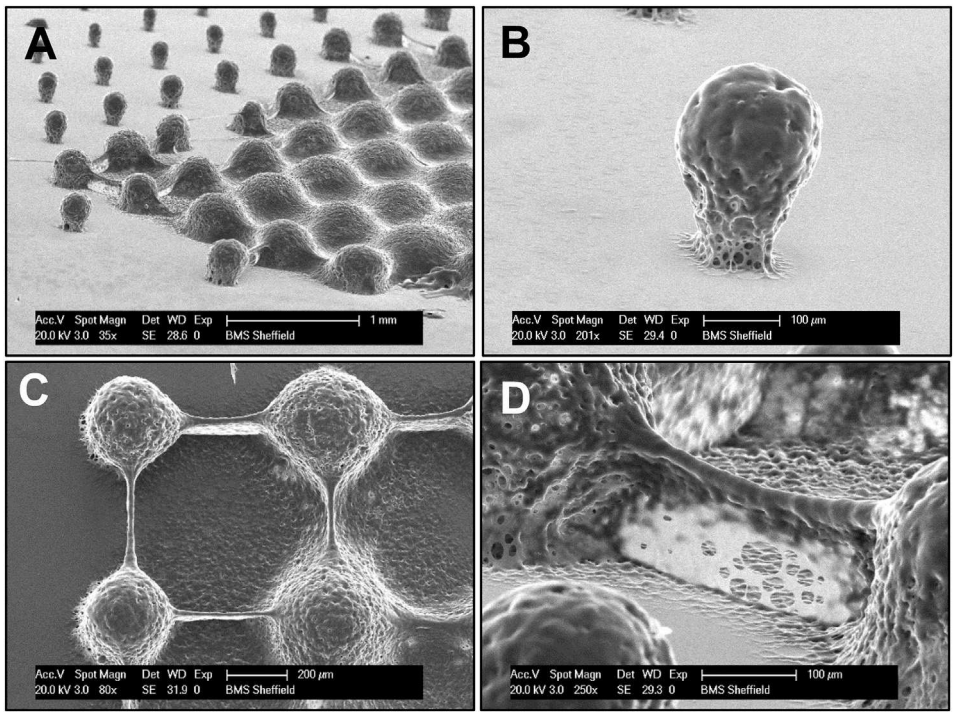

Fig. 2. A) SEM image of part of the PolyHIPE protrusion spot array showing the isolated protrusions gradually increasing in size and merging together. The laser pulse time was increased in increments of 0.01 s until a final exposure time of 1.3 s and a constant spacing of 700 μm was used for all the protrusions. Scale bar 1 mm. (B) A single PolyHIPE protrusion produced by pulsing the laser, a surface skin can be observed around the object. Scale bar 100 μm. (C) Top view of polymer bridges that have formed between 4 PolyHIPE protrusions that can be seen in image A. Scale bar 200 μm. (D) Side view of the polymer bridge seen in image A and C. A thin layer of polymer skin can be seen covering both the polymer bridge down towards the glass surface. Scale bar 100 μm.

process results in the emulsion acting as a diffuse light source, with a radius-dependent intensity profile emanating from the focal spot that results in a gradual reduction in the degree of polymerisation as the distance increases from the focal spot. When the partially polymerised regions surrounding two separate PolyHIPE irradiation spots overlap, a connecting polymer bridge forms between them. The polymer bridge forms along the straight path that is the shortest distance between the two irradiation spots. The surface skin surrounding the PolyHIPE is also formed by this partially cross-linked polymer as it collapses around the fabricated structure.

3.3. Incorporation of light-absorbers can reduce surface skin formation

Due to the undesirable nature of this surface skin, different strategies to remove the surface skin were explored. Acid degradation of the surface skin was examined by a 12-hour submersion in piranha solution. However, this treatment did not result in the removal of the surface skin (data not shown). In addition to the use of oxidisers such as a 0.1 M solution of potassium permanganate ($KMnO_4$), or air plasma (2 h exposure) to etch the surface were explored. However, these approaches were also ineffective.

An alternative strategy to degrading the skin post-fabrication was to try and minimise its initial formation through the incorporation of a UV light-absorber or a radical scavenger into the HIPE. To test this, the radical scavenger 4-methoxyphenol (MEHQ) or the light-absorber UV-234 were added to the HIPE at 1 wt%. To quantify their effects on the achievable resolution, a series of single spots were irradiated with a 0.1 s dwell time in a straight line, with the spacing gradually decreased by 10 μm increments until the PolyHIPE protrusions connected. The distance between them was recorded at that point. This was repeated for different laser dwell times ranging from 0.1 to 1 s in increments of 0.1 s and the values were plotted for the original emulsion together with the emulsion with MEHQ and UV-234 (Fig. 3A). Additionally, the achieved feature size (measured as diameter) for the different resins and laser irradiation was recorded and plotted (Fig. 3B). Interestingly, both the diameter of the protrusion and the minimal obtainable distance between features has a strong linear correlation with curing exposure time. The addition of these additives achieved a reduction in the minimal feature size and an improvement in obtainable resolution. The addition of MEHQ showed a small improvement in resolution and minimal achievable feature size. UV-234 demonstrated a much higher improvement and the maximum reduction in feature spacing when using the light-absorber was significantly greater (500 to 240 μm) (Fig. 3).

The feature resolution and fabricated structure quality is clearly increased when UV-234 is incorporated into the HIPE resin (Fig. 4). In comparison to the standard resin, the incorporation of the UV-234 light-absorber mitigates the formation of the surface skin, revealing an open pore surface. Furthermore, a marked improvement in print resolution can also be observed, as the features written with the standard IBOA resin began to overlap when their distance was 500 μm, whilst the features written with the IBOA+UV-234 resin began to overlap at 200 μm.

3.4. UV-234 is not cytotoxic in non-degradable polymers

Although the incorporation of UV-234 can significantly improve the printing resolution of PolyHIPEs, within the field of 3D cell culture and tissue engineering, this is irrelevant if its presence causes cell death. To assess the potential cytotoxicity of UV-234, the murine osteoblast cell line MLO-A5 was cultured on 4-layer woodpile scaffolds fabricated from IBOA or IBOA+UV-234 PolyHIPEs. The achievable fibre spacing was determined by SEM image analysis and cell metabolic activity (RR) assays were performed weekly over a 28-day period. Furthermore, the mechanical properties of the bulk PolyHIPE material with and without UV-234 were compared to assess whether its inclusion affected the stiffness (Fig. 5).

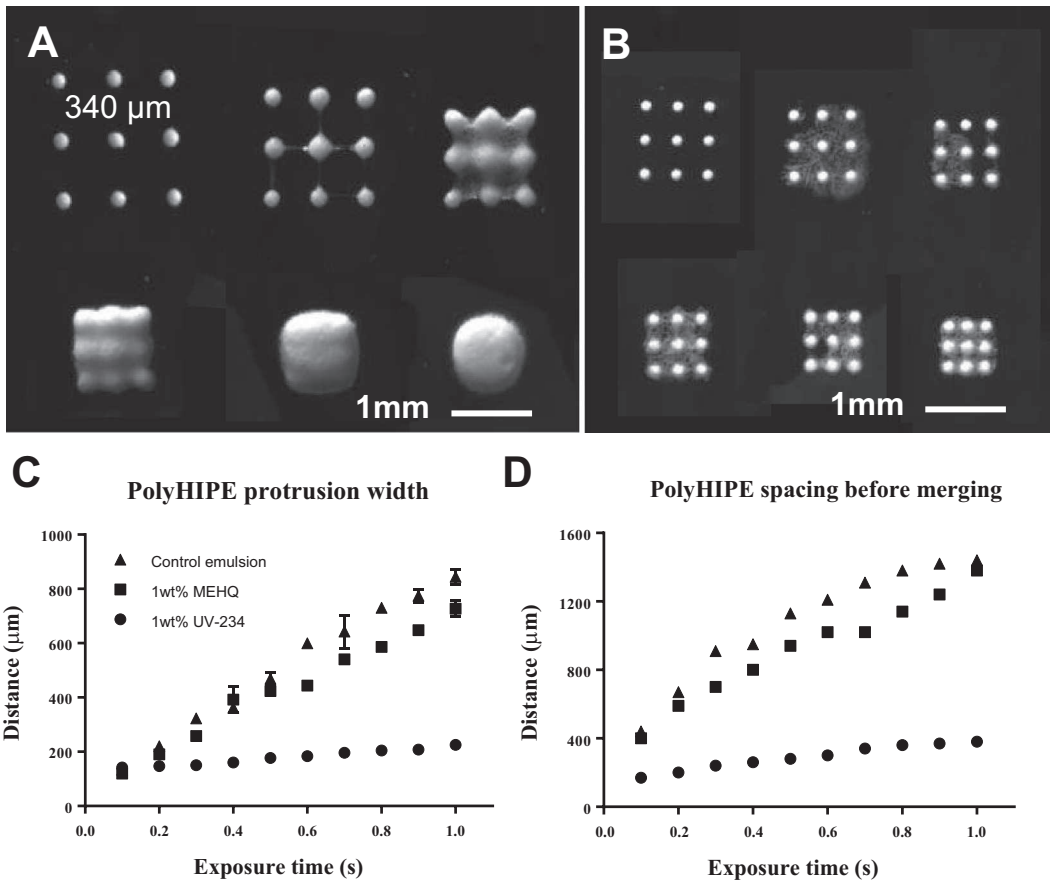

Fig. 3. (A)–(B) Composite light microscope images of PolyHIPE protrusions in a 3 by 3 square lattice. (A) The original emulsion, and (B) emulsion with 1 wt% UV-234. (A) The spacing between the protrusions in the square lattice is reduced by 100 μm going from 700 to 200 μm. (B) The spacing between the protrusions is reduced by 40 μm from 400 to 240 μm. All samples were produced with a laser exposure of 0.2 s, at 5 mW. (C)–(D) Scatter graph showing the distance between the PolyHIPE protrusions when they started to merge together for the emulsion with no light absorber, 1 wt% MEHQ radical scavenger and 1 wt% UV-234 light-absorber. (D) Scatter graph showing the diameter of the PolyHIPE protrusions at different exposure durations.

Incorporation of UV-234 allowed scaffold fibres to be written approximately 200 μm closer together without a skin forming between them. Furthermore, side skin formation appeared to be reduced by the presence of UV-234, but was not eliminated entirely. The inclusion of UV-234 had no significant effect on the Young's Modulus of the PolyHIPE, demonstrating that its inclusion will not change the material stiffness and any subsequent cellular response. To control for scaffold surface area when evaluating cytotoxicity, the fibre spacing in the IBOA-UV-234 scaffold was kept the same as in the IBOA scaffold. There was no significant difference in between cell metabolic activity on the IBOA and IBOA+UV-234 scaffolds at any time point (Fig. 5E), indicating that the addition of UV-234 had no detectable cytotoxic effect. The metabolic activity of the MLO-A5 cells increased during the first week of the experiment, indicating that the cells were proliferating. The plateau from day 7 onwards indicates that the cells on the scaffold had reached confluence.

3.5. In scaffolds of similar architecture, multiscale porosity improves cellular performance

To evaluate whether the inclusion of a multiscale porosity in a woodpile architecture is beneficial, PolyHIPE scaffolds were compared to the

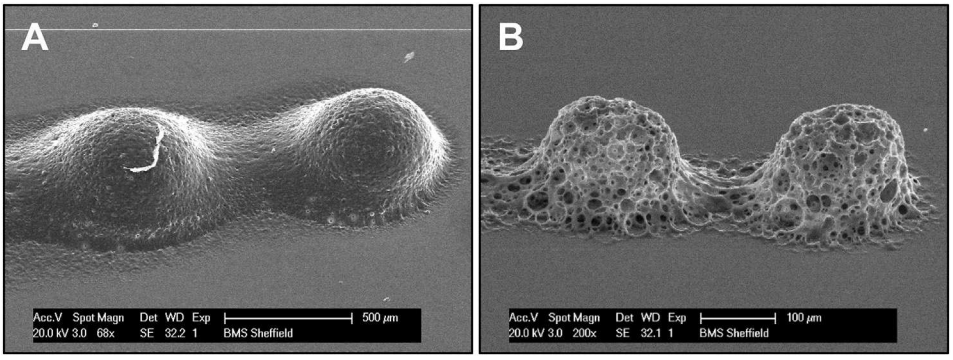

Fig. 4. SEM images of the PolyHIPE protrusions. (A) Two standard IBOA emulsion-based PolyHIPE protrusions with a closed surface skin around them and excess curing between them. (B) The same IBOA PolyHIPE but with the incorporation of 1% UV-234. An open surface porosity and significantly reduced extraneous curing are clearly visible despite the distance between the protrusions being significantly smaller.

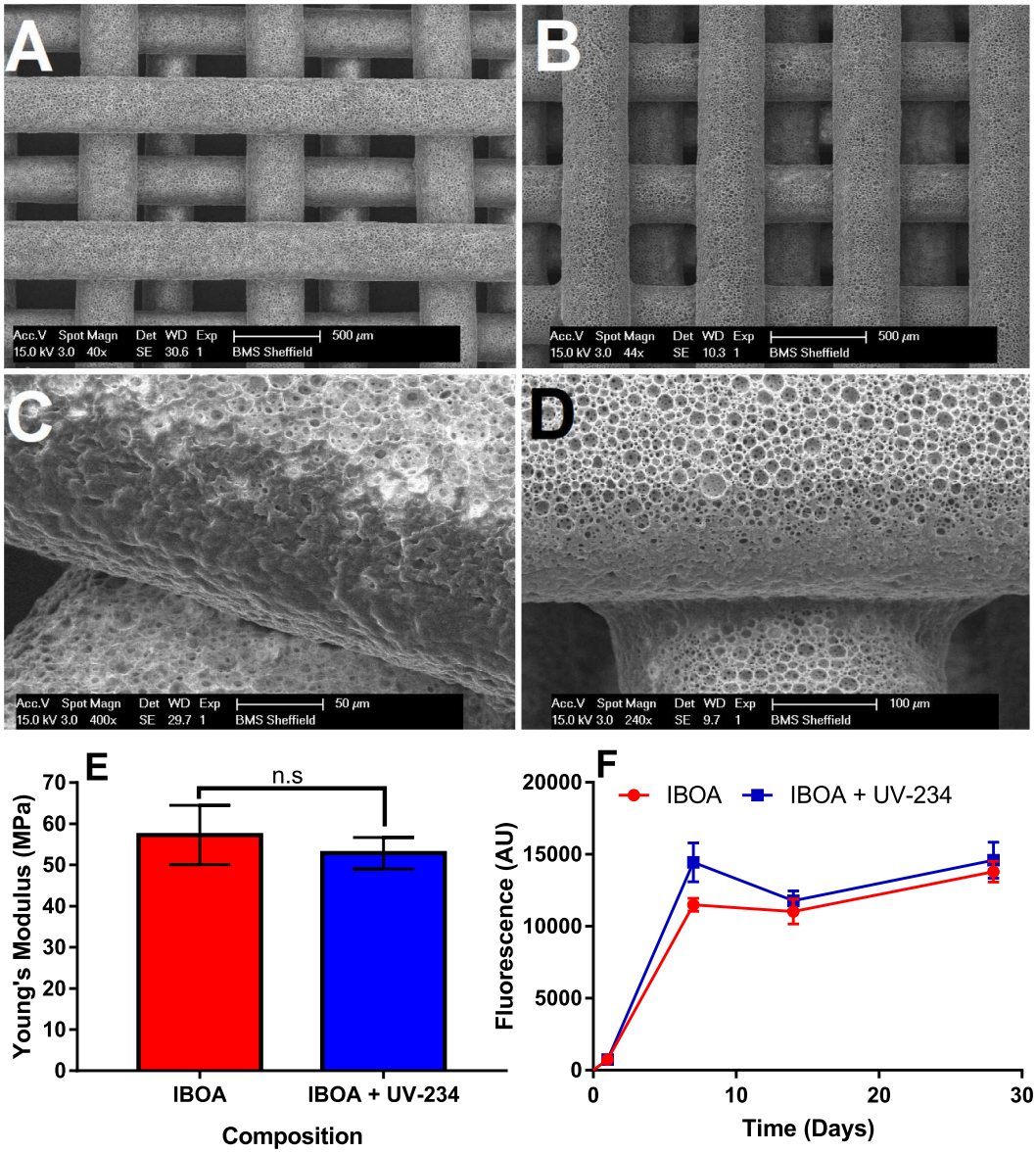

Fig. 5. SEM images of an (A&C) IBOA and (B&D) IBOA+UV-234 woodpile scaffold. Minimum achievable fibre spacing is reduced in scaffolds fabricated from IBOA+UV-234. Side skin formation is reduced but not eliminated. (E) Incorporation of UV-234 had no significant effect on the Young's modulus of the PolyHIPE ($n = 8$). (F) Metabolic activity for IBOA scaffolds with and without UV-234 over a 28-day period. No significant difference at any time point indicating no cytotoxic effect of UV-234 ($n = 6$).

3D Insert™-PCL (Biotek, 3D Biotek, USA), a commercially available woodpile scaffold with a similar architecture that has non-porous fibres. Both scaffolds have a fibre diameter and spacing of approximately 300 μm and a diameter of 13–14 mm; however, the PCL-based Biotek scaffold has six layers whereas the IBOA-based PolyHIPE has only 4. Importantly, only the PolyHIPE scaffold has microporous fibres. Cellular performance was compared by culturing each scaffold with 25,000 MLO-A5 for 28 days, assessing metabolic activity each week and calcium and collagen deposition on days 21 and 28. The Biotek scaffold was seeded according to manufacturer instructions (Fig. 6).

Although cells proliferated on both scaffolds, metabolic activity increased significantly faster on the PolyHIPE and reached a plateau, indicating confluence (Fig. 6A). Fig. 6B illustrates a typical cross-section of the 6-layer Biotek scaffold indicating a strut size of 300 μm and an inter-strut distance of 300 μm; there was also variation in fibre geometry and spacing. (Fig. 6B). Mineralisation as indicated by ARS was significantly higher on the PolyHIPE scaffold ($p < 0.001$) and mineral distribution was uniform throughout the scaffold, rather than patchy as observed on the Biotek scaffold (Fig. 6C & D). Collagen deposition followed the same pattern as mineralisation, and was 4–5× less on the Biotek scaffold (Fig. 6E).

4. Discussion

Porous matrices based on PolyHIPEs have been readily used in the last 10 years as scaffolds to study 3D cell culture due to the ease with which a porous structure can be made and the tunability of the resulting microporosity to optimise cell ingrowth. The application of these scaffolds for 3D cell culture has been highly successful, yielding a commercially available scaffold for 3D cell culture (ALVATEX®). This scaffold is a flat porous polystyrene disk, 200 μm in thickness with 40 μm pore sizes that is optimised for in vitro cell culture. To increase the application of these PolyHIPE materials towards more complex 3D cell culture there has been a recent research effort to combine this emulsion templating with 3D printing approaches such as stereolithography or materials extrusion to build structures with a hierarchy of pore sizes.

Additive manufacturing of PolyHIPEs via stereolithography produces a surface skin on the outer surface that could impede cell ingrowth by

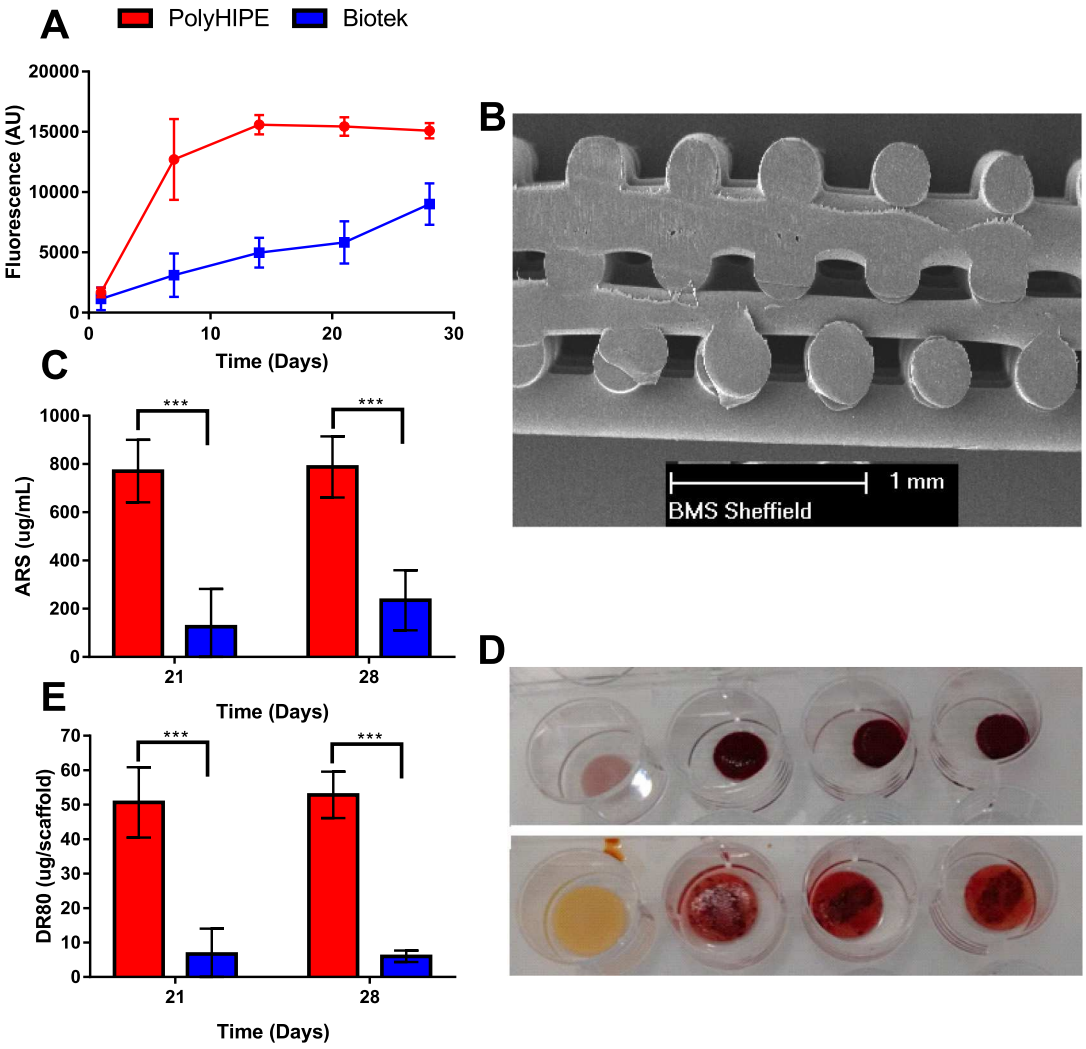

Fig. 6. Comparison of the PolyHIPE and Biotek woodpile scaffolds. (A) metabolic activity of MLO-A5 increased significantly faster on the PolyHIPE scaffold ($n = 12$). (B) The Biotek woodpile architecture was inconsistent and fibres were not always above the spacing of the layer below. (C&D) mineral deposition and distribution was significantly greater and more uniform in the PolyHIPE scaffold ($n = 6$) (E) as was collagen deposition (n = 6). *** = $p < 0.001$.

acting as a physical barrier and therefore negating the advantages of using the HIPE as a template. The internal porosity of the PolyHIPE is unaffected by this unwanted polymerisation on the exterior and remains an open-pored network (Fig. 1), a finding which is in agreement with our previous work [3]. Stereolithography of emulsions to build materials with hierarchical porosity is currently an emerging research area and presently little detailed information is available on how to optimise the resolution and mitigate closed surface porosity in these structures. This study reports on how to optimise the structure resolution and obtain open surface porosity via adding a light absorber to the resin.

The occurrence of a closed surface skin layer has previously been reported when performing bulk polymerisation of PolyHIPEs, with the skin forming at the emulsion-mould interface [7,35]. This is comparable to the closed-pore skin layer often observed when curing against a mould in other porous material fabrication techniques, e.g. supercritical fluid-foaming [36]. This surface layer can easily be removed from monoliths by cutting after polymerisation; however, this approach is unsuitable for any complex structures produced by additive manufacturing. Therefore, an approach that minimises its formation is required, and to achieve this, understanding the mechanism by which it is formed is essential. It was observed that no surface skin is present when the HIPE is polymerised with an emulsion/air interface (Fig. 1). Furthermore, the top surface of the woodpile PolyHIPE lines were open pored whilst their sides had a surface skin, which indicates that it is the transition from cured to non-cured polymer that is causing the localised collapse of the PolyHIPE surface resulting in the surface skin (Fig. 5).

This study strongly indicates that UV light scattering within the HIPE is a major contributing factor in the formation of the surface skin, as it directly relates to the boundary layer of partially polymerised polymer surrounding the PolyHIPE. The HIPE scatters light, evident from the opaque white colour when the emulsion is produced, and this is caused by the mismatch between the refractive index between two phases in an emulsion [37]. The scattering of the UV light from its initial focal point within the emulsion produces an intensity gradient that decreases in energy outwards from the initial point of exposure. This results in a continual decrease in the degree of polymerisation as the distance from the focal spot increases, resulting in the transition from cured to non-cured polymer. This transition results in the production of a mechanically weak polymer on the surface of the PolyHIPE that cannot support its own structure but is sufficiently-crosslinked to be resistant to the washing solvent. The subsequent collapse of this layer during washing creates the closed surface skin layer.

To evaluate whether this mechanism of skin formation was correct, lines were cured by stereolithography but the surrounding uncured pre-polymer was not washed away. Instead, the residual HIPE bulk polymerised and the resulting structure cross-sectioned (Supplementary Fig. S3). As no surface skin or indication of the initial polymerised lines were seen in these images, this approach confirmed that the

cured outer surface that would typically collapse and form the skin layer was still supported by the emulsion droplets after fabrication, demonstrating that the collapse does not occur until solvent washing.

During the drying of the PolyHIPE, capillary forces generated by the solvent evaporating causes the collapse of the polymer on the surface. Freeze drying could be used to prevent surface collapse by these forces, but this is an involved process requiring long waiting times [38]. In our single spot exposure experiment (Fig. 2), all the protrusions possessed a surface skin which indicated that varying the UV light exposure alone does not eliminate the skin layer, and it was only with the addition of a light-absorber that no skin was formed on the PolyHIPE protrusion (Fig. 4).

The addition of the UV light-absorber UV-234 eliminated the closed surface skin effect (Fig. 4), and had a very notable effect on the reduction of a single PolyHIPE feature size in comparison to the addition of MEHQ radical scavenger or plain IBOA-HIPE (Fig. 3). A surface skin surrounded the plain IBOA-HIPE and the MEHQ-HIPE, suggesting that the surface skin relates to the UV light scattering. The addition of UV-234-like absorbers (from the Tinuvin Carboprotect product family) has been previously reported to improve the resolution of stereolithography printing of a HIPE; however, there was no mention of a surface skin [2]. The light scattering has been highlighted in previous papers on projection-based stereolithography as the major contributing factor in reducing the resolution of a written object [39–41]. It is common practice to use a light-absorber to improve the resolution as it decreases the cure depth by absorbing the incident light [42]. Other UV absorbers can be used for this, e.g. Tinuvin 327 has a broad UV absorbance with a peak of 40% at 365 nm [42], while Tinuvin P absorbs between 250 and 400 nm. When a typical 1 wt% is added to the monomer both the solidification width and depth of the exposed areas can be decreased [41].

Without any light-absorber, the written features, when placed at the correct distance, often present polymer bridges in between them (Fig. 2C and D). The proposed mechanism for the polymer bridges is the overlapping of the partially polymerised polymer that surrounds the PolyHIPE protrusions. This causes additional crosslinking of the monomer which is sufficient to form a polymer bridge connecting adjacent protrusions. The overlap between these partially polymerised regions can be controlled by varying the amount of UV light exposure (Fig. 2), or changing the distance between adjacent protrusions (Fig. 3). In all cases there appears to be an outer boundary limit that determines if polymer bridges will form. The overlapping of sub-activated radical regions has been previously reported as the cause behind connecting polymer bridges by high resolution two photon polymerisation which is caused by radical diffusion [43]. The radical diffusion scale is of minor importance in the production of our sub-millimetre scale features. Nevertheless, they share visual similarities to the polymer bridges reported in this paper, and are both exposure and distance dependent.

The PolyHIPE scaffolds used in this study were produced by scanning stereolithography which cures the polymer in a single focal point. The important parameters are the scan speed and laser intensity. In this experiment we used a low intensity (1–5 mW) picosecond pulsed UV source, which also restricted our maximum write speed. Using higher power lasers should enable a significant increase in write speed. Taking this into account our experiment could still create features at a write speed of 3 mm/s. Faster write speeds created a line of polymer residue that had no internal structure due to insufficient amount of polymerisation. These write speeds (0.5–5 mm/s) were also previously reported by our group [3]. Additionally, these HIPE resins can be used in combination with projection stereolithography, which uses typically a spatial light modulator-based dynamic mask [2,3] which can drastically decrease the processing time as a single layer is polymerised at the same time. In contrast, materials extrusion speeds up to 10 mm/s have been reported [15], but with lower resolution i.e. line widths of 600 μm. Our previous publication reported structures with feature resolution of 330 μm [4] via stereolithography and this study shows that this resolution can be improved upon to 200 μm by inclusion of a light-absorber (Fig. 4). Length scales are crucial to achieve optimal cell ingrowth within the scaffolds as nutrient and oxygen diffuse up to 100–200 μm within a micrometre porous scaffold and any cells further away from a nutrient/oxygen source will likely undergo hypoxic necrosis [44].

Inclusion of UV-234 successfully reduced the formation of the side skin on the scaffold fibres, although it did not completely mitigate its development. Despite this, a greater proportion of the scaffold surface having an open porosity will be beneficial to diffusion-based processes, such as nutrient and waste diffusion, as well as facilitating greater cell ingrowth which in turn permits more continuous neo-tissue formation throughout the scaffold. Importantly, the inclusion of UV-234 had no significant effects on cell metabolic activity over a long culture period, indicating that its inclusion was not cytotoxic, and that it did not leach out of the polymer over time. This is in agreement with the work of Zhang, et al., how found that the inclusion of UV-234 did not have a negative effect on the growth of HUVECs and NIH-3T3 cells cultured on a non-degradable poly(ethylene glycol) diacrylate (PEGDA, M_w 700 g/mol) scaffold [45]. However, whether this remains the case when a biodegradeable, more clinically relevant polymer is used would need to be assessed prior to its consideration for use in vivo.

To assess whether the theorised benefits of the inclusion of a microporosity within the fibre were valid, PolyHIPE scaffolds were compared to Biotek 3D Insert™-PCL scaffolds which possess a similar macrostructure but lack the inherent micropores of the PolyHIPE material. MLO-A5 were able to proliferate significantly faster over the PolyHIPE scaffolds, resulting in them reaching confluence sooner and depositing significantly greater amounts of mineralised extracellular matrix. Synthesis of the bone-like matrix was also more evenly distributed over the PolyHIPE scaffold, showing that cells were able to quickly grow throughout the entire structure. The benefits of fibre microporosity seen here are in agreement with the findings of other groups, who found that it improves cell ingrowth in PCL-based scaffolds [46,47].

In addition to the benefits of enhanced diffusion-based processes, another potential reason for this enhanced cellular response when micropores are present is that the cells are able to develop a more physiologically relevant morphology in comparison non-porous fibres. On smooth fibres, cells are likely to retain a similar morphology to when they a cultured on a flat, planar surface such as a tissue culture plate. However, when cells are cultured on a surface with features and pores that are a similar size to themselves, they are able to attach to the surface and develop a morphology that is more similar to that observed in vivo, and this has been shown improver osteogenic differentiation and osteoblast activity [48–50]. For future work we foresee that the addition of calcium phosphate-based components, such as hydroxyapatite, may increase the bone-matrix deposition. The benefits of this composite material approach have been shown with extrusion based woodpile scaffolds [26] and the PolyHIPE based structure [29,30]. Nevertheless, effects of incorporating another element into the emulsion on UV-light scattering and surface skin formation would need to be addressed if a stereolithography-based manufacturing approach is taken.

5. Conclusion

To conclude, UV-234 (or Tinuvin®234), a UV light absorber, was found to improve the fabrication of PolyHIPE structures by stereolithography (vat photopolymerisation) through two mechanisms. First, it reduced the formation of an undesirable surface skin that has a closed porosity, negating the benefits of the PolyHIPE material. Second, it increased the resolution of the fabrication technique by permitting smaller PolyHIPE features to be fabricated with greatly decreased spacing. The addition of UV-234 was found to be non-cytotoxic, and when PolyHIPE scaffolds were compared to scaffolds with similar architecture but without microporosity, they were found to support superior MLO-A5 osteoblast proliferation and matrix production.

This study demonstrates how the simple incorporation of a UV light absorber into the prepolymer can greatly improve the printing resolution of PolyHIPEs by stereolithography, allowing for bespoke, highly customisable substrates to be fabricated. This finding continues to exemplify the excellent candidacy of PolyHIPE materials for use as tissue engineering and cell culture substrates in comparison to standard, non-emulsified polymers.

Acknowledgements

We acknowledge funding from the Engineering and Physical Sciences Research Council (Grant no. EP/L505055/1 and EP/N509735/1) and Biotechnology and Biological Sciences Research Council (Grant no. BB/F016840/1).

Data availability statement

The raw/processed data required to reproduce these findings cannot be shared at this time due to technical or time limitations.

Appendix A. Supplementary data

Supplementary data to this article can be found online at https://doi.org/10.1016/j.matdes.2018.06.061.

References

[1] B. Dhandayuthapani, Y. Yoshida, T. Maekawa, D.S. Kumar, Polymeric scaffolds in tissue engineering application: a review, Int. J. Polym. Sci. 2011 (2011).
[2] M. Sušec, S.C. Ligon, J. Stampfl, R. Liska, P. Krajnc, Hierarchically porous materials from layer-by-layer photopolymerization of high internal phase emulsions, Macromol. Rapid Commun. 34 (2013) 938–943.
[3] D.W. Johnson, C. Sherborne, M.P. Didsbury, C. Pateman, N.R. Cameron, F. Claeyssens, Macrostructuring of emulsion-templated porous polymers by 3D laser patterning, Adv. Mater. 25 (2013) 3178–3181.
[4] R. Owen, C. Sherborne, T. Paterson, N.H. Green, G.C. Reilly, F. Claeyssens, Emulsion templated scaffolds with tunable mechanical properties for bone tissue engineering, J. Mech. Behav. Biomed. Mater. 54 (2016) 159–172.
[5] Q.L. Loh, C. Choong, Three-dimensional scaffolds for tissue engineering applications: role of porosity and pore size, Tissue Eng. B Rev. 19 (6) (2013) 485–502.
[6] J. Naranda, M. Sušec, U. Maver, L. Gradišnik, M. Gorenjak, A. Vukasović, A. Ivković, M.S. Rupnik, M. Vogrin, P. Krajnc, Polyester type polyHIPE scaffolds with an interconnected porous structure for cartilage regeneration, Sci. Rep. 6 (2016).
[7] N.R. Cameron, High internal phase emulsion templating as a route to well-defined porous polymers, Polymer 46 (5) (2005) 1439–1449.
[8] A. Richez, H. Deleuze, P. Vedrenne, R. Collier, Preparation of ultra-low-density microcellular materials, J. Appl. Polym. Sci. 96 (6) (2005) 2053–2063.
[9] J.M. Williams, A.J. Gray, M.H. Wilkerson, Emulsion stability and rigid foams from styrene or divinylbenzene water-in-oil emulsions, Langmuir 6 (2) (1990) 437–444.
[10] J.L. Robinson, R.S. Moglia, M.C. Stuebben, M.A.P. McEnery, E. Cosgriff-Hernandez, Achieving interconnected pore architecture in injectable polyHIPEs for bone tissue engineering, Tissue Eng. A 20 (5–6) (2014) 1103–1112.
[11] S.D. Kimmins, N.R. Cameron, Functional porous polymers by emulsion templating: recent advances, Adv. Funct. Mater. 21 (2) (2011) 211–225.
[12] M.S. Silverstein, Emulsion-templated porous polymers: a retrospective perspective, Polymer 55 (1) (2014) 304–320.
[13] A.-j. Wang, T. Paterson, R. Owen, C. Sherborne, J. Dugan, J.-m. Li, F. Claeyssens, Photocurable high internal phase emulsions (HIPEs) containing hydroxyapatite for additive manufacture of tissue engineering scaffolds with multi-scale porosity, Mater. Sci. Eng. C 67 (2016) 51–58.
[14] S. Nicholas, D. Prachi, W. Michael, C.-H. Elizabeth, Fabrication of biomimetic bone grafts with multi-material 3D printing, Biofabrication 9 (2) (2017), 025020.
[15] N.A. Sears, P.S. Dhavalikar, E.M. Cosgriff-Hernandez, Emulsion inks for 3D printing of high porosity materials, Macromol. Rapid Commun. 37 (16) (2016) 1369–1374.
[16] A. Malayeri, C. Sherborne, T. Paterson, S. Mittar, I.O. Asencio, P.V. Hatton, F. Claeyssens, Osteosarcoma growth on trabecular bone mimicking structures manufactured via laser direct write, Int. J. Bioprinting 2 (2) (2016).
[17] W. Busby, N.R. Cameron, C.A.B. Jahoda, Tissue engineering matrixes by emulsion templating, Polym. Int. 51 (10) (2002) 871–881.
[18] R.S. Moglia, M. Whitely, P. Dhavalikar, J. Robinson, H. Pearce, M. Brooks, M. Stuebben, N. Cordner, E. Cosgriff-Hernandez, Injectable polymerized high internal phase emulsions with rapid in situ curing, Biomacromolecules 15 (8) (2014) 2870–2878.
[19] D.W. Johnson, C.R. Langford, M.P. Didsbury, B. Lipp, S.A. Przyborski, N.R. Cameron, Fully biodegradable and biocompatible emulsion templated polymer scaffolds by thiol-acrylate polymerization of polycaprolactone macromonomers, Polym. Chem. 6 (41) (2015) 7256–7263.
[20] N. Sears, P. Dhavalikar, M. Whitely, E. Cosgriff-Hernandez, Fabrication of biomimetic bone grafts with multi-material 3D printing, Biofabrication 9 (2) (2017), 025020.
[21] M.W. Hayman, K.H. Smith, N.R. Cameron, S.A. Przyborski, Enhanced neurite outgrowth by human neurons grown on solid three-dimensional scaffolds, Biochem. Biophys. Res. Commun. 314 (2) (2004) 483–488.
[22] G. Akay, M.A. Birch, M.A. Bokhari, Microcellular polyHIPE polymer supports osteoblast growth and bone formation in vitro, Biomaterials 25 (18) (2004) 3991–4000.
[23] S.J. Hollister, Porous scaffold design for tissue engineering, Nat. Mater. 4 (7) (2005) 518–524.
[24] I. Cooperstein, M. Layani, S. Magdassi, 3D printing of porous structures by UV-curable O/W emulsion for fabrication of conductive objects, J. Mater. Chem. C 3 (9) (2015) 2040–2044.
[25] T. Patrício, M. Domingos, A. Gloria, U. D'Amora, J.F. Coelho, P.J. Bártolo, Fabrication and characterisation of PCL and PCL/PLA scaffolds for tissue engineering, Rapid Prototyp. J. 20 (2) (2014) 145–156.
[26] M. Domingos, A. Gloria, J. Coelho, P. Bartolo, J. Ciurana, Three-dimensional printed bone scaffolds: the role of nano/micro-hydroxyapatite particles on the adhesion and differentiation of human mesenchymal stem cells, Proc. Inst. Mech. Eng. H J. Eng. Med. 231 (6) (2017) 555–564.
[27] L. Germain, C.A. Fuentes, A.W. van Vuure, A. des Rieux, C. Dupont-Gillain, 3D-printed biodegradable gyroid scaffolds for tissue engineering applications, Mater. Des. 151 (2018) 113–122.
[28] Y. Luo, Y. Li, X. Qin, Q. Wa, 3D printing of concentrated alginate/gelatin scaffolds with homogeneous nano apatite coating for bone tissue engineering, Mater. Des. 146 (2018) 12–19.
[29] J.L. Robinson, M.A.P. McEnery, H. Pearce, M.E. Whitely, D.J. Munoz-Pinto, M.S. Hahn, H. Li, N.A. Sears, E. Cosgriff-Hernandez, Osteoinductive PolyHIPE foams as injectable bone grafts, Tissue Eng. A 22 (5–6) (2016) 403–414.
[30] A. Lee, C.R. Langford, L.M. Rodriguez-Lorenzo, H. Thissen, N.R. Cameron, Bioceramic nanocomposite thiol-acrylate polyHIPE scaffolds for enhanced osteoblastic cell culture in 3D, Biomater. Sci. 5 (10) (2017) 2035–2047.
[31] R. Owen, C. Sherborne, G.C. Reilly, F. Claeyssens, Data for the analysis of PolyHIPE scaffolds with tunable mechanical properties for bone tissue engineering, Data Brief 5 (2015) 616–620.
[32] A. Barbetta, N.R. Cameron, Morphology and surface area of emulsion-derived (PolyHIPE) solid foams prepared with oil-phase soluble porogenic solvents: span 80 as surfactant, Macromolecules 37 (9) (2004) 3188–3201.
[33] G. Tetteh, A.S. Khan, R.M. Delaine-Smith, G.C. Reilly, I.U. Rehman, Electrospun polyurethane/hydroxyapatite bioactive scaffolds for bone tissue engineering: the role of solvent and hydroxyapatite particles, J. Mech. Behav. Biomed. Mater. 39 (2014) 95–110.
[34] A. Sittichockechaiwut, A.M. Scutt, A.J. Ryan, L.F. Bonewald, G.C. Reilly, Use of rapidly mineralising osteoblasts and short periods of mechanical loading to accelerate matrix maturation in 3D scaffolds, Bone 44 (5) (2009) 822–829.
[35] I. Pulko, P. Krajnc, Open cellular reactive porous membranes from high internal phase emulsions, Chem. Commun. (37) (2008) 4481–4483.
[36] Y. Reinwald, R.K. Johal, A.M. Ghaemmaghami, F. Rose, S.M. Howdle, K.M. Shakesheff, Interconnectivity and permeability of supercritical fluid-foamed scaffolds and the effect of their structural properties on cell distribution, Polymer 55 (1) (2014) 435–444.
[37] T. Zhang, Q. Guo, Isorefractive high internal phase emulsion organogels for light induced reactions, Chem. Commun. 52 (24) (2016) 4561–4564.
[38] M.-H. Ho, P.-Y. Kuo, H.-J. Hsieh, T.-Y. Hsien, L.-T. Hou, J.-Y. Lai, D.-M. Wang, Preparation of porous scaffolds by using freeze-extraction and freeze-gelation methods, Biomaterials 25 (1) (2004) 129–138.
[39] S. Zissi, A. Bertsch, J.Y. Jézéquel, S. Corbel, D.J. Lougnot, J.C. Andre, Stereolithography and microtechniques, Microsyst. Technol. 2 (2) (1996) 97–102.
[40] L.-H. Han, G. Mapili, S. Chen, K. Roy, Projection microfabrication of three-dimensional scaffolds for tissue engineering, J. Manuf. Sci. Eng. 130 (2) (2008), 021005.
[41] J.S. Choi, H.-W. Kang, I.H. Lee, T.J. Ko, D.-W. Cho, Development of micro-stereolithography technology using a UV lamp and optical fiber, Int. J. Adv. Manuf. Technol. 41 (3) (2009) 281–286.
[42] J.-W. Choi, R.B. Wicker, S.-H. Cho, C.-S. Ha, S.-H. Lee, Cure depth control for complex 3D microstructure fabrication in dynamic mask projection microstereolithography, Rapid Prototyp. J. 15 (1) (2009) 59–70.
[43] S.H. Park, T.W. Lim, D.-Y. Yang, N.C. Cho, K.-S. Lee, Fabrication of a bunch of sub-30-nm nanofibers inside microchannels using photopolymerization via a long exposure technique, Appl. Phys. Lett. 89 (17) (2006), 173133.
[44] J. Rouwkema, N.C. Rivron, C.A. van Blitterswijk, Vascularization in tissue engineering, Trends Biotechnol. 26 (8) (2008) 434–441.
[45] A.P. Zhang, X. Qu, P. Soman, K.C. Hribar, J.W. Lee, S. Chen, S. He, Rapid fabrication of complex 3D extracellular microenvironments by dynamic optical projection stereolithography, Adv. Mater. 24 (31) (2012) 4266–4270.
[46] F.E. Wiria, K.F. Leong, C.K. Chua, Y. Liu, Poly-ε-caprolactone/hydroxyapatite for tissue engineering scaffold fabrication via selective laser sintering, Acta Biomater. 3 (1) (2007) 1–12.
[47] W.Y. Yeong, N. Sudarmadji, H.Y. Yu, C.K. Chua, K.F. Leong, S.S. Venkatraman, Y.C.F. Boey, L.P. Tan, Porous polycaprolactone scaffold for cardiac tissue engineering fabricated by selective laser sintering, Acta Biomater. 6 (6) (2010) 2028–2034.
[48] G.C. Reilly, A.J. Engler, Intrinsic extracellular matrix properties regulate stem cell differentiation, J. Biomech. 43 (1) (2010) 55–62.
[49] M.M. Stevens, J.H. George, Exploring and engineering the cell surface interface, Science 310 (5751) (2005) 1135–1138.
[50] E. Knight, B. Murray, R. Carnachan, S. Przyborski, Alvetex®: Polystyrene Scaffold Technology for Routine Three Dimensional Cell Culture, 3D Cell Culture: Methods and Protocols, 2011 323–340.